



UNIVERSITY OF LEEDS

This is a repository copy of *On the interpretation of reflectivity data from lipid bilayers in terms of molecular-dynamics models*.

White Rose Research Online URL for this paper:
<http://eprints.whiterose.ac.uk/110051/>

Version: Accepted Version

Article:

Hughes, AV, Ciesielski, F, Kalli, AC orcid.org/0000-0001-7156-9403 et al. (4 more authors) (2016) On the interpretation of reflectivity data from lipid bilayers in terms of molecular-dynamics models. *Acta Crystallographica Section D: Structural Biology*, 72 (12). pp. 1227-1240.

<https://doi.org/10.1107/S2059798316016235>

Reuse

Unless indicated otherwise, fulltext items are protected by copyright with all rights reserved. The copyright exception in section 29 of the Copyright, Designs and Patents Act 1988 allows the making of a single copy solely for the purpose of non-commercial research or private study within the limits of fair dealing. The publisher or other rights-holder may allow further reproduction and re-use of this version - refer to the White Rose Research Online record for this item. Where records identify the publisher as the copyright holder, users can verify any specific terms of use on the publisher's website.

Takedown

If you consider content in White Rose Research Online to be in breach of UK law, please notify us by emailing eprints@whiterose.ac.uk including the URL of the record and the reason for the withdrawal request.



eprints@whiterose.ac.uk
<https://eprints.whiterose.ac.uk/>



On the interpretation of reflectivity data from lipid bilayers in terms of molecular-dynamics models

Arwel V. Hughes, Fillip Ciesielski, Antreas C. Kalli, Luke A. Clifton, Timothy R. Charlton, Mark S. P. Sansom and John R. P. Webster

Acta Cryst. (2016). **D72**, 1227–1240



IUCr Journals

CRYSTALLOGRAPHY JOURNALS ONLINE

Copyright © International Union of Crystallography

Author(s) of this paper may load this reprint on their own web site or institutional repository provided that this cover page is retained. Republication of this article or its storage in electronic databases other than as specified above is not permitted without prior permission in writing from the IUCr.

For further information see <http://journals.iucr.org/services/authorrights.html>

On the interpretation of reflectivity data from lipid bilayers in terms of molecular-dynamics models

Arwel V. Hughes,^{a*} Fillip Ciesielski,^a Antreas C. Kalli,^b Luke A. Clifton,^a
 Timothy R. Charlton,^a Mark S. P. Sansom^b and John R. P. Webster^a

^aISIS Pulsed Neutron Source, Rutherford Appleton Laboratory, Harwell OX11 0QX, England, and ^bDepartment of Biochemistry, University of Oxford, Oxford OX1 3QU, England. *Correspondence e-mail: arwel.hughes@stfc.ac.uk

Received 28 June 2016

Accepted 12 October 2016

Edited by P. Langan, Oak Ridge National Laboratory, USA

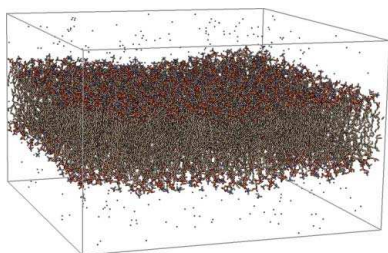
Keywords: molecular dynamics; biomembranes; reflectivity.

Neutron and X-ray reflectivity of model membranes is increasingly used as a tool for the study of membrane structures and dynamics. As the systems under study become more complex, and as long, all-atom molecular-dynamics (MD) simulations of membranes become more available, there is increasing interest in the use of MD simulations in the analysis of reflectometry data from membranes. In order to perform this, it is necessary to produce a model of the complete interface, including not only the MD-derived structure of the membrane, but also the supporting substrate and any other interfacial layers that may be present. Here, it is shown that this is best performed by first producing a model of the occupied volume across the entire interface, and then converting this into a scattering length density (SLD) profile, rather than by splicing together the separate SLD profiles from the substrate layers and the membrane, since the latter approach can lead to discontinuities in the SLD profile and subsequent artefacts in the reflectivity calculation. It is also shown how the MD-derived membrane structure should be corrected to account for lower than optimal coverage and out-of-plane membrane fluctuations. Finally, the method of including the entire membrane structure in the reflectivity calculation is compared with an alternative approach in which the membrane components are approximated by functional forms, with only the component volumes being extracted from the simulation. It is shown that using only the fragment volumes is insufficient for a typical neutron data set of a single deuteration measured at several water contrasts, and that either weighting the model by including more structural information from the fit, or a larger data set involving a range of deuterations, are required to satisfactorily define the problem.

1. Introduction

The phospholipid bilayer is the basic structural unit of biological membranes. Most cellular activities involve membrane interactions at some point, be it in the simplest case transport of agents across the membrane into the cells, or processes that occur in the membrane region itself, either internally within the cell or externally in its interaction with the wider environment (Sachs & Engelman, 2006). There is therefore great interest in studying membrane processes to better understand the role of this region in cell behaviour. In recent years, there has been extensive use of both X-ray and neutron reflectivity to probe the structures, dynamics and interactions of cell membranes (Wacklin, 2010). Reflectivity offers ångstrom-resolution structural characterization of bilayer systems, and in the case of neutrons allows selective deuteration to probe specific regions or components of the membrane (Penfold, 2002).

Since reflection is by definition a surface-sensitive technique, such studies necessarily involve the study of model membrane mimics deposited on surfaces. A variety of



approaches have been employed to fabricate model membranes on surfaces, the simplest of which involves simply depositing bilayers directly onto substrates, usually silicon or mica, by either direct fusion of vesicles or by Langmuir–Blodgett (LB) or Langmuir–Schaeffer (LS) methods (Richter *et al.*, 2006). These directly supported membranes are structurally phospholipid bilayers, but their behaviour is impacted by the proximity of the substrate, which has a constraining effect on the mobility of the membrane components (Xing & Faller, 2008). Various approaches have been proposed to reduce this substrate influence, including pre-coating the substrates with polymer cushions (Majewski *et al.*, 1998), fabricating multiple layers (Katsaras & Gutberlet, 2001) or mimicking the balance of forces observed in multilamellar vesicles by depositing bilayers onto existing phospholipid coatings (Hughes *et al.*, 2008, 2014). The latter approach leads to membranes which remain associated with the substrate but separated from it by substantial cushions of water owing to entropic effects (Hughes *et al.*, 2008, 2014; Helfrich, 1973; Daillant *et al.*, 2005; Fragneto *et al.*, 2012; Clifton *et al.*, 2015; Daulton, 2015). These floating supported bilayers (FSBs) have the advantage of a high degree of structural control afforded by the Langmuir–Blodgett methodology used in their construction, but the separation from the substrate greatly reduces its constraining effect. Supported bilayers have been used to probe a number of phenomena from nucleotide–membrane interactions to the behaviour of novel antimicrobials to fundamental membrane biophysics (Dabkowska *et al.*, 2015; Daillant *et al.*, 2005; Fragneto *et al.*, 2012; Clifton *et al.*, 2015; Daulton, 2015).

Traditionally, model membranes for reflectivity studies have been simple one-component or two-component phospholipid bilayers, with the compositions varying slightly in terms of lipid charge or chain unsaturation to probe specific electrostatic interactions or the effects of changes in fluidity. More recently, advances in the fabrication methodologies of floating membranes have allowed more complex membranes to be probed. Therefore, rather than simply using a simple phospholipid bilayer, mimics of specific membrane types such as the Gram-negative bacterial outer membrane (Clifton *et al.*, 2015) or raft-forming membranes (Daulton, 2015) are being developed. As the complexity of the samples increases, so too does the demand on the data-analysis methodologies used to extract structural information from the resulting reflection data.

A reflectivity profile is a probe of the entire interfacial region, and except under very specific conditions, the sample of interest (*i.e.* in this case the bilayer) and any other surface layers or coatings must be accounted for in the interpretation of the data. Usually, the interfacial region is modelled by ‘resampling’ the density profile across the interface into a number of distinct layers (Abeles, 1950). Thus, a simple phospholipid bilayer could be represented by a series of layers, each of which is identified with the head groups or the hydrophilic tails, and also layers would be included to represent any other surface coatings such as polymers, self-assembled monolayers, metal coatings and so on. The

reflectivity is then calculated from these models by transfer-matrix approaches (Abeles, 1950).

This layers approach works well for simple systems. In these cases, layers can be clearly identified as corresponding to specific regions of the interface (*i.e.* such as the head group), and any changes or behaviours seen can then be interpreted in this context. However, as the complexity of the samples increases, then so does the strain put on the approximations made in the modelling. Specifically, for more complex systems, it becomes increasingly ambiguous as to how many layers should be appropriately included in the models to describe the systems under study. Thus, for lipopolysaccharides, or large membrane proteins, for example, the specification of a layer model and the definition of its limits increasingly become an influence on the results, introducing concerns of bias in the analysis.

For these reasons, there has long been interest in using more rigorous modelling strategies in the interpretation of reflection data, in particular from molecular-dynamics (MD) simulations of membranes (Heinrich & Lösche, 2014; Koldsø *et al.*, 2014). MD simulations of membranes have become increasingly sophisticated in recent years, involving large-scale, long-duration simulations of complicated multicomponent protein-containing membranes (Kaszuba *et al.*, 2015). As such, the resulting structures can offer significant insights into the structures of complex biological systems, and including this information in the analysis of reflection data could greatly enhance the interpretation of reflection experiments. Thus, for example, if a simulation suggested more than one possible orientation for an integral or peripheral protein domain, then reflectivity data could be used as an independent screen of these candidate structures to determine which of the plausible set in fact exists, but with reduced selection bias compared with layer resampling.

The ‘refractive index’ in a scattering experiment, known as the scattering length density (SLD), is a function of the atomic composition per unit volume. Methods for converting all-atom simulations or membranes into SLD profiles are well known, and have been extensively employed in the interpretation of diffraction (Wiener & White, 1992; Tristram-Nagle *et al.*, 1998) or small-angle scattering measurements (Kučerka *et al.*, 2008, 2012), either with neutrons or X-rays. Some examples are also known for reflectivity, mainly for monolayers (Schalke & Lösche, 2000; Schalke *et al.*, 2000), but also with some reported for bilayers (Hughes *et al.*, 2002).

The most common approach to including information from MD simulations into the analysis of scattering data does not in fact usually rely on converting the results of the simulation into an SLD profile directly, but instead extracts certain information from the simulations, usually component volumes; these are then used as inputs into structural models which build the SLD profile in functional form (Wiener & White, 1992; Tristram-Nagle *et al.*, 1998; Kučerka *et al.*, 2008, 2012; Schalke & Lösche, 2000; Schalke *et al.*, 2000; Hughes *et al.*, 2002).

Thus, for example, positional distributions of membrane components might be approximated as Gaussians or

combinations of error functions, and the component volumes are then used to convert these into SLD profiles. The advantage of this approach, known as ‘compositional space refinement’ (CSR), is that the volumes may be used in other systems where the same fragments are present without needing to carry out new simulations for each case. Thus, for example, volumes extracted for the fragments of DPPC from a pure DPPC bilayer simulation may be used for any mixed system where DPPC is present. Similarly, if a membrane structure changes

in response to an external stimulus (such as pressure or temperature, for example), then using movable distributions can allow these changes to be followed without the need to produce a new simulation for each set of conditions. The disadvantage is that whilst the approximation of using Gaussians or similar is very good for the head-group components of simpler lipids, the appropriate functional forms from more complicated inclusions such as proteins and so on are not always clear.

An alternative to the functional approach is to take the entire simulation (converted into an SLD) as a unit, and then use this as part of a larger model to build up the full SLD profile required for the particular geometry of the experiment in question (Darré *et al.*, 2015). This approach has the advantage that there are then no operator decisions to be made in terms of the shapes of particular fragment distributions, as these are extracted from the simulations directly. It has the disadvantage, however, of requiring a new simulation for each data set analysed, but this is becoming less of an issue as the ready availability of computing power makes this a feasible option in many cases. However, in order to use this approach for reflectivity, there are also difficulties in terms of how to include the simulated structure into the larger model of the entire interface without introducing artefacts into the final calculation.

The main purpose of this paper is firstly to make explicit how *whole* MD membrane structures should be included into a reflectivity model without introducing artefacts caused by incorrect splicing between the modelled membrane SLD and the SLD profile of the rest of the interface. We show that this should be performed by first producing a model of the occupied volume across the entire interface, and subsequently ‘space-filling’ the model with water to give a smooth profile, rather than by splicing together the individual SLDs of the membrane and supporting layers, since the latter can introduce artefacts into the structural calculation. Secondly, we also show how the calculated membrane SLD should be corrected to account for incomplete coverage and out-of-plane membrane fluctuations. We show that this method gives excellent agreement with a simple test model of a fluid-phase DPPC floating bilayer. Finally, we then compare the performance of the this ‘whole-simulation’ approach with the more common CSR model, where the membrane submolecular fragments are modelled as Gaussians, with their positions and widths as fitting parameters and with the only information taken from the MD simulations being the volumes of the individual fragments. We show that in the reflectivity case,

whilst CSR can indeed model the membrane structure accurately, using only the fragment volumes is insufficient for the data set used here (a typical result from a reflectivity experiment), and that it is necessary to either include additional information on fragment positions, or alternatively a larger data set including extensive selective deuteration to reliably model the membrane. The extension of this approach to more complex mixed-membrane systems is also discussed.

2. Experimental

2.1. MD simulations of DPPC

The bilayer was constructed using a self-assembly coarse-grained molecular dynamics (SA-CG-MD) simulation protocol. For the CG-MD simulation the Martini forcefield (v2.1) was used (Marrink *et al.*, 2007). For this simulation 115 coarse-grained DPPC molecules were randomly added in a simulation box along with CG water particles and counterions. The simulation was run for 100 ns after an initial 150 steps of energy minimization. At the end of the SA-CG-MD simulation a bilayer was formed in the *xy* plane of the box. Subsequently, the simulation box was replicated (3×3) in the *x* and *y* dimensions using the *genconf* command in *GROMACS*, thus creating a bilayer with 1035 coarse-grained DPPC molecules. The system, which also contained coarse-grained water molecules and counter-ions, was energy-minimized for 150 steps followed by 100 ns of production simulation. This coarse-grained protocol resulted in an equilibrated DPPC bilayer with 1035 DPPC molecules. Coarse-grained (CG) to atomistic (AT) conversion was performed using the *CG2AT* protocol as described previously by Stansfeld and coworkers (Tristram-Nagle *et al.*, 1998). Atomistic molecular-dynamics simulations were performed using the GROMOS96 53a6 force field. The DPPC lipid parameters were taken from Kukul (2009). These parameters were shown to reproduce experimental measurements for a DPPC bilayer, for example the area per lipid and deuterium order parameter of the acyl chains. The SPC water model was used and counter-ions were added to neutralize the system. The Parrinello–Rahman barostat (Parrinello & Rahman, 1981) and the V-rescale thermostat (Bussi *et al.*, 2007) were used for pressure and temperature coupling, respectively. The *LINCS* algorithm (Hess *et al.*, 1997) was used to constrain bond lengths, and the particle mesh Ewald (PME) algorithm (Darden *et al.*, 1993) was used to model long-range electrostatic interactions. The temperature was set to 323 K. After the conversion to an atomistic representation, the system was energy-minimized and a short equilibration simulation of 1 ns with the phosphate atoms of the lipids restrained was performed. A production atomistic simulation was run for 500 ns with a time step of 2 fs.

2.2. Fabrication and characterization of DPPC floating bilayers

ω -Thiolipid [1-oleoyl-2-(16-thiopalmitoyl)-*sn*-glycero-3-phosphocholine; Avanti Polar Lipids] was dissolved at

1 mg ml⁻¹ in chloroform/methanol (4:1), dried as a film in a glass tube and resuspended in 1% octylglucopyranoside (OG; Sigma), 50 mM Tris pH 8.0 (OG buffer). Immediately prior to use, tris(2-carboxyethyl)phosphine-HCl (TCEP) was added to a final concentration of 1 mM. The gold surfaces were cleaned by sonication in 2% Hellmanex solution (Hellma GmbH), rinsed and then sonicated in 1% sodium dodecyl sulfate (SDS) solution. The cleaned surfaces were immersed in the ω -thio-lipid/OG solution for 2 h at 50°C. The surfaces were removed from the lipid solution, cleaned again in SDS and re-immersed in the lipid solution for a further 2 h. Finally, the surfaces were removed from the coating solution, washed with SDS, rinsed with ultrapure water (UPW; Millipore; 18.2 m Ω cm⁻¹) and dried under nitrogen.

The LB/LS depositions were carried out using a purpose-built LB trough (Nima Technology, Coventry, England). The trough has a large, deep dipping well to accommodate the horizontally oriented silicon crystals during the Schaeffer transfer. The trough was cleaned and filled with UPW. DPPC (Avanti Polar Lipids) was dissolved in chloroform at approximately 1 mg ml⁻¹, and 300 μ l was spread onto the cleaned water surface. After waiting for 15 min to allow the monolayer to equilibrate, the monolayer was compressed at 50 cm² min⁻¹ to 30 mN m⁻¹. For the first LB transfer, the compression was carried out with the substrate already immersed in the trough. After reaching the target pressure, the substrate was withdrawn upwards through the monolayer at 5 mm min⁻¹, with the trough running in constant-pressure mode.

For LS transfers, a clean neutron reflection cell was placed in the trough before it was filled. After filling the trough, the monolayer was spread and compressed to the required pressure, and the substrate was mounted horizontally on the dipper such that its gold face was parallel to the water surface. The tilt of the substrate was adjusted using a motor-controlled levelling stage, such that the substrate and the water were exactly parallel. The substrate was then pushed through the interface at a speed of 5 mm min⁻¹ and then sealed in the neutron cell while still underwater, as described previously (Daillant *et al.*, 2005; Fragneto *et al.*, 2012; Clifton *et al.*, 2015; Daulton, 2015).

2.3. Polarized neutron reflectivity

NR measurements were carried out on the POLREF white-beam reflectometer at the Rutherford Appleton Laboratory, Oxfordshire, England. NR measures the neutron reflection as a function of the angle and/or wavelength (λ) of the beam relative to the sample. The reflected intensity was measured as a function of the momentum transfer q_z [$q_z = (4\pi\sin\theta)/\lambda$, where λ is the wavelength and θ is the incident angle]. White-beam instruments probe a wide area of q_z space at a single angle of reflection owing to the use of a broad neutron spectrum. To obtain reflectivity data across a q_z range of ~ 0.01 – 0.3 , glancing angles of 0.5, 1.0 and 2.3° were used ($\lambda = 2$ – 12 Å).

Sample cells were sealed, removed from the LB trough and mounted on a variable-angle sample stage in the reflectometer. The samples are placed in a magnetic field. The two spin orientations result in two distinct nSLDs for the permalloy layer but an unchanged nSLD for the rest of the sample. The inlet to the liquid cell was connected to a liquid-chromatography pump (L7100 HPLC pump, Merck, Hitachi) which was programmed to remotely change the solution H/D mix in the sample cells. In this work, the bilayer structure was analysed in two solution isotopic contrasts, either 100% D₂O or 100% H₂O, and measured at 50°C.

2.4. Data fitting

An average structure was constructed by summation of the individual time slices of the production MD run. Each slice was centred on the terminal methyl groups of the bilayer before averaging. The resulting MD simulations box, which was 175.85 \times 175.85 \times 108.263 Å (in x , y and z , respectively, with the membrane lying in the xy plane), was divided into 0.12 Å slices along z , leading to 917 slices in total in the simulation box. The atoms of each lipid head group were grouped into choline (C₆H₁₃N), phospho (PO₄), glycerol (C₂H₅) or carbonyl (C₂O₂) ‘quasimolecular’ fragments (Wiener & White, 1992; Tristram-Nagle *et al.*, 1998; Kučerka *et al.*, 2008, 2012; Schalke & Lösche, 2000; Schalke *et al.*, 2000; Hughes *et al.*, 2002; Petrache *et al.*, 1997), and the alkyl chains (CH₂) and terminal methyls (CH₃–) were also grouped to give six distributions in total for each lipid. The number of occurrences of each group within each slice were counted and histogrammed to yield number density distributions, from which SLD and volume profiles were obtained as described previously (Petrache *et al.*, 1997). These were then combined with profiles from the remainder of the interface to build the full SLD profiles as described in the next section. The SLD and volume profiles were then used as part of a ‘custom xy profile’ in the *RasCAL* fitting environment (<https://sourceforge.net/projects/rscl/>). The model was fitted to the experimental data using a Bayesian Markov chain Monte Carlo algorithm (Haario *et al.*, 2006).

3. Results

3.1. Direct use of a complete MD structure in producing an SLD profile

The approach that we consider is to take a molecular-dynamics structure of a membrane, extract average positional distributions of the membrane components from the simulations and then combine these with a model of the supporting layers to build a continuous scattering length density (SLD) profile that we then compare with the measured data. It should be emphasized that in building the SLD profile we take the complete simulated membrane structure as a unit, and that this is distinct to the usual approach of reconstituting the membrane structure from functional forms (usually Gaussians), which we consider in §4.

A typical MD structure for fluid-phase DPPC obtained as described in §2 is shown in Fig. 1(a). Following Petrache *et al.* (1997), the structure is divided into a series of quasimolecular fragments representing groups of atoms, in an analogous way to how a coarse-grained model might be developed. In this case, the head groups are divided into four regions representing carbonyl, glycerol, phospho and choline regions. The overlapping terminal methyl regions of each lipid are grouped together into a single distribution, and the ‘alkyl’ regions (representing the methylene groups of the chains) are treated as a single unit. Additionally, the bulk waters on each side of the membrane are also included, and all the distributions are summed together to give the overall ‘total’ structure, as shown in Fig. 1(b).

Fig. 1(c) shows each distribution as probability distributions of the fragment positions. To obtain these, the simulation box

of the membrane is divided into slices of thickness Δz (where the z axis is defined as normal to the bilayer plane), and the number of occurrences of each particular group within each slice, $N(z)$, is counted and histogrammed. The number density is then

$$n(z) = \frac{N(z)}{V_s} = \frac{N(z)}{A_c \cdot \Delta z}, \quad (1)$$

where V_s is the volume of the slice, which is given by the slice thickness times the projected area of the unit cell into the bilayer plane (A_c). The volume of each component can be calculated as shown previously by Petrache *et al.* (1997) by imposing a condition of space-filling (*i.e.* void volumes are neglected) such that

$$V_1 n_1(z) + V_2 n_2(z) + \dots + V_n n_n(z) = 1 \quad (2)$$

over all z , where V_ξ are the component volumes and $V_\xi n_\xi(z) \equiv p_\xi(z)$ are the probability distributions shown in Fig. 1(a). In practice, the component volumes are obtained by iteratively minimizing $\sum_z [\sum_\xi p_\xi(z) - 1]^2$ with V_ξ as the fitting parameters (Darré *et al.*, 2015).

The reflectivity is eventually calculated from the scattering length density (SLD), which is obtained from the distributions

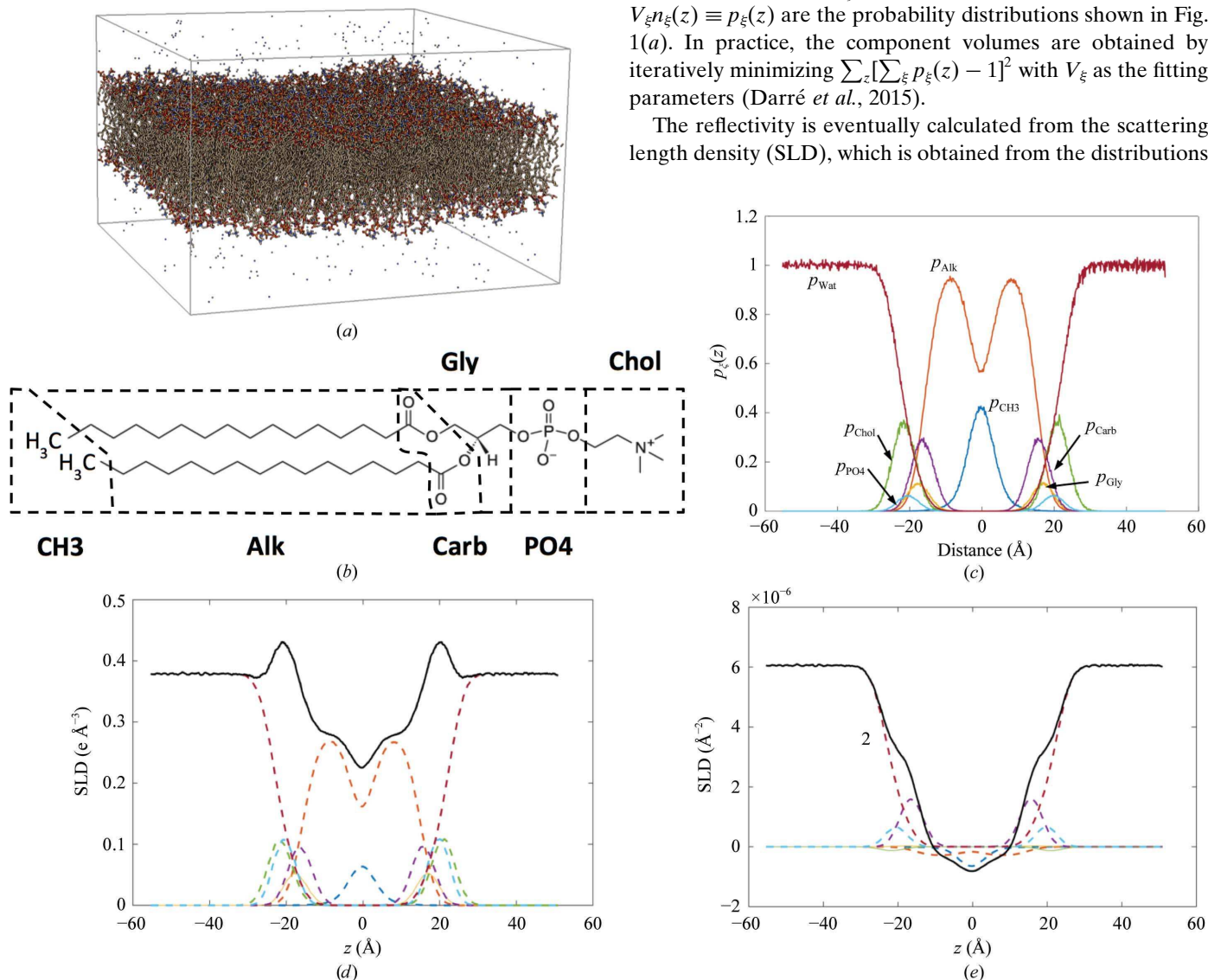


Figure 1

(a) MD simulation of a fluid-phase DPPC bilayer. (b) Specification of the ‘quasimolecular fragments’ used in parsing DPPC. Each molecule is divided into six fragments: ‘CH3’ (C_2H_6), ‘Alk’ [$(\text{CH}_2)_n$], ‘Carb’ (C_2O_4), ‘PO4’ (PO_4), ‘Gly’ (C_3H_5) and ‘Chol’ ($\text{C}_5\text{H}_{12}\text{N}$). (c) Probability distributions of the fragments from fluid-phase DPPC obtained from the MD simulation described in §2, calculated according to (1), (2) and (3). (d) shows an X-ray SLD profile obtained from the distributions in (c), and (e) shows the neutron case against D_2O .

shown in Fig. 1(a) by multiplying by the relevant scattering length of each group, s , so that

$$s_{\xi} = \begin{cases} \sum_i n_i b_i & \text{for neutrons} \\ n_e r_o & \text{for X-rays} \end{cases}, \quad (3)$$

where b_i is the bound coherent scattering length for the i th type of atom for the neutron case, and n_e is the number of electrons and r_o is the classical Compton wavelength for X-rays. For each distribution, the scattering length density (SLD) is then given by

$$\rho(z) = \frac{p_{\xi}(z) \cdot s_{\xi}}{V_{\xi}}. \quad (4)$$

An X-ray SLD profile calculated from Fig. 1(c) is shown in Fig. 1(d), and the neutron case (against D₂O) is shown in Fig. 1(e).

In a reflectivity measurement, the bilayer does not scatter in isolation and is by the nature of the technique supported on a

substrate, and the contribution of the substrate to the SLD profile must also be included. In the case of the supported bilayer considered in this example, this requires contributions from the silicon substrate, the oxide layer and the supporting self-assembled monolayer (SAM), as can be seen from the cartoon structure of the system shown in Fig. 2(a). The simplest way of building up an SLD profile whilst including the MD SLD is to then model the SLDs of the supporting layers and then simply splice these to the calculated bilayer SLD profile. This is shown in Fig. 2(b), and a problem becomes immediately apparent. If the values of the SLDs at the edges of the two contributions do not match (as is easily and often the case when the effects of roughness are considered) then a discontinuity is introduced at the splicing point, as highlighted by the arrow in Fig. 2(a). Although this appears as a small feature in the profile, the significance of the problem becomes more apparent when we remember that reflectivity is a function not of the SLD profile itself, but of the Fourier transform of the square of its gradient (Penfold, 2002) and, as can be seen in the plot of $|\mathrm{d}\rho(z)/\mathrm{d}z|^2$ shown in Fig. 2(c), the discontinuity in this case becomes the dominant feature. In other words, any reflectivity calculated from Fig. 2(b) is substantially caused by an artefact rather than the sample structure.

If the volume of each fragment is known, this problem can be overcome by building the SLD profile in terms of the occupied volume rather than by splicing the individual SLDs. The probabilities can be equivalently viewed as volume fractions, since the slice volumes appear in the denominator of (1) and the component volumes in (2), with $\sum_{\xi} p_{\xi}(z) = 1$ then indicating full occupancy of a given slice, and a number less than unity indicating that unfilled volume exists at that point in z . In the case of Fig. 1, the volume occupied includes the water molecules from the simulations, but in constructing the whole profile we omit these distributions and consider the volume occupied by the bilayer *except* for the water, and similarly for the SAM layers. To splice in terms of volume, the procedure is first to calculate the total occupied volume across the whole of the interface (*i.e.* including the SAM and the substrate) neglecting water.

In this example, the SAM model is constructed using the compositional space refinement approach by using Gaussian distributions to represent $p_{\xi}(z)$, as described previously (Schalke & Lösche, 2000; Schalke *et al.*, 2000; Hughes *et al.*, 2002). Essentially, rather than using distributions obtained from modelling to describe the positions of the quasimolecular fragments of the head group, the probability distributions are assumed to be Gaussians, and their positions relative to the SAM tails and their widths (represented by an overall SAM roughness) become fitting parameters (Schalke & Lösche, 2000; Schalke *et al.*, 2000; Hughes *et al.*, 2002). The SAM tail region, and any lower layers of the substrates, are modelled by simple step functions. These distributions are treated as probability distributions in the same way as those derived from the simulations in Fig. 1, and the SLD is calculated by the application of (3) and (4). To perform this, component volumes are clearly required, and in the case of the SAM, literature volumes for DPPC are taken (Armen *et al.*, 1998).

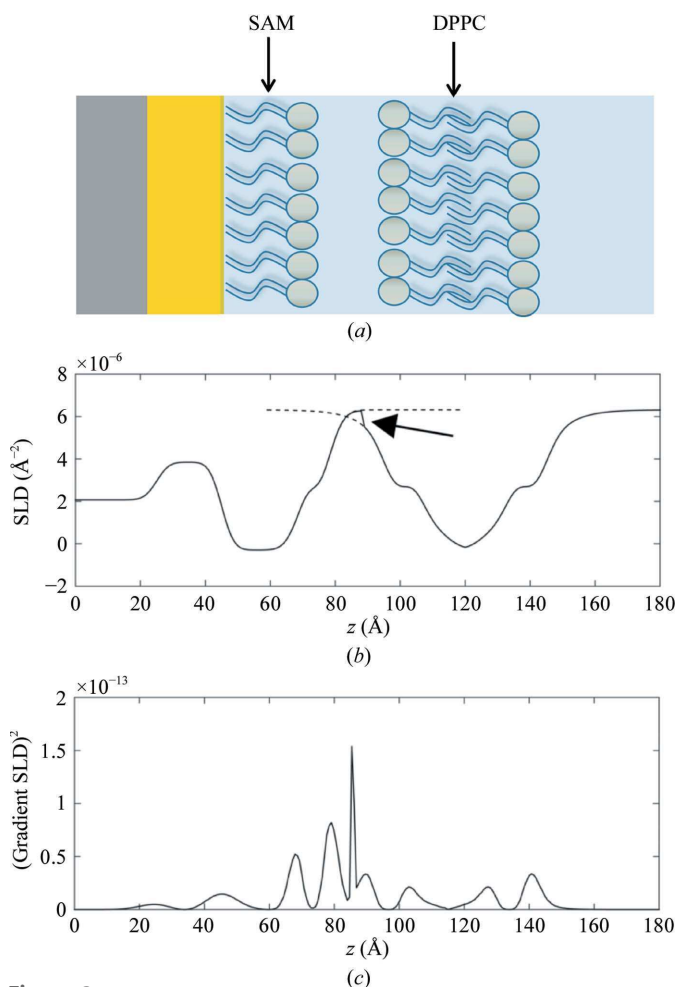


Figure 2
(a) Cartoon structure of the floating bilayer example considered in this work. The membrane is supported by a grafted phospholipid coating and is separated from the substrate by a water cushion. (b) Direct splicing of MD profiles calculated separately for the lower layers and the bilayer can introduce discontinuities at the splicing point, as indicated by the arrow. (c) Squared gradient of the SLD profile shown in (b), which illustrates that under these conditions the discontinuity becomes a dominant feature introducing artefacts into any subsequent reflectivity calculation.

Once the probability distributions for all components of the interface are known, the total sum over all of the distributions may be easily obtained. If we assume that any remaining volume must be occupied by water in the submerged system (*i.e.* the space-filling criterion), then the quantity $1 - \sum_{\xi} p_{\xi}(z)$ will give the remaining water distribution across the interface. The salient point is that the water distribution is calculated with reference to all of the volumes across the *entire* interface, and by doing so any splicing at the edges of individual SLD profiles is avoided, thus eliminating discontinuities.

The procedure is illustrated in Fig. 3, which shows the construction of the complete SLD profile for the DPPC floating bilayer. Fig. 3(a) shows the $p(z)$ for the DPPC bilayer from the MD data in Fig. 1 on the right, whilst the CSR SAM structure calculated from the Gaussian distributions and the substrate step functions are on the left. The thick blue line in Fig. 3(a) is then the volume unfilled by the model, which is the overall distribution for the water, and as long as there is no ‘overfilling’ of the model (*i.e.* an unphysical model in which the sum of the required volumes within a slice exceeds V_s , leading to a negative available volume for water) then the water distribution is always continuous. To obtain the complete scattering length density profile, the number densities are multiplied by the relevant scattering lengths, and the water distribution by $(2n_D + n_O)/V_w$, where n_D and n_O are the neutron scattering lengths of deuterium and oxygen, respectively, and V_w is the volume of a water molecule, which is taken as 30.2 \AA^3 (Armen *et al.*, 1998). The substrate distributions are simply multiplied by their expected SLDs to give the complete profile shown in Fig. 3(b). The profile is continuous and there are no artefacts in the gradient, as shown in Fig. 3(c).

In addition to determining the volume occupancy of the individual components across the interface, there is still some work to do in order to complete the SLD profile. Floating bilayers do so because they display out-of-plane fluctuations, leading to an entropically driven repulsion between the membrane and the lower layers (Helfrich, 1973). The effect of this is to ‘smear’ out the SLD profile of the membrane, and in order to account for these displacements we convolute the profile obtained from the MD calculations with a Gaussian, the width of which represents the level of displacement. This is illustrated in Fig. 4(a), which shows the DPPC SLD profile as the solid line, with the dashed and dotted–dashed lines showing the effect of a Fourier convolution of the distributions with Gaussians of width 3 and 7 Å, respectively.

An additional complication is that the coverage of the membrane may not be complete, with defects in the form of holes present. The overall SLD profile from the bilayer region will then be a scaled sum of the SLD profile of a full bilayer and that of the solvent. We introduce a fractional bilayer coverage parameter, C_B , where a value of zero means that the membrane is absent, whereas a value of unity reflects a complete, defect-free bilayer. To correct for lower than optimal coverage, the procedure is then to simply scale the $\sum_{\xi} p_{\xi}(z)$ for the membrane. This is shown in Fig. 4(b), where the solid lines are total probabilities and the dotted lines show the free ‘volume’ [*i.e.* $1 - \sum_{\xi} p_{\xi}(z)$]. The pair of curves

labelled ‘I’ are for full occupancy, and those marked as ‘II’ are for the case of $C_B = 0.6$. In the latter case of incomplete coverage, it should be noted that the water distribution no longer decreases to zero in the centre of the membrane, and so this automatically results in water-filled defects, as would be expected. In addition, it is necessary to scale the SLD profile [as well as $N(z)$], and the effect of this is shown in Fig. 4(c). The overall result is shown in Fig. 4(d), which shows the complete SLD profile for the DPPC membrane, produced with the ‘as simulated’ MD distribution (solid line); the dotted line shows the same profile, but with a convolution of 5 Å and

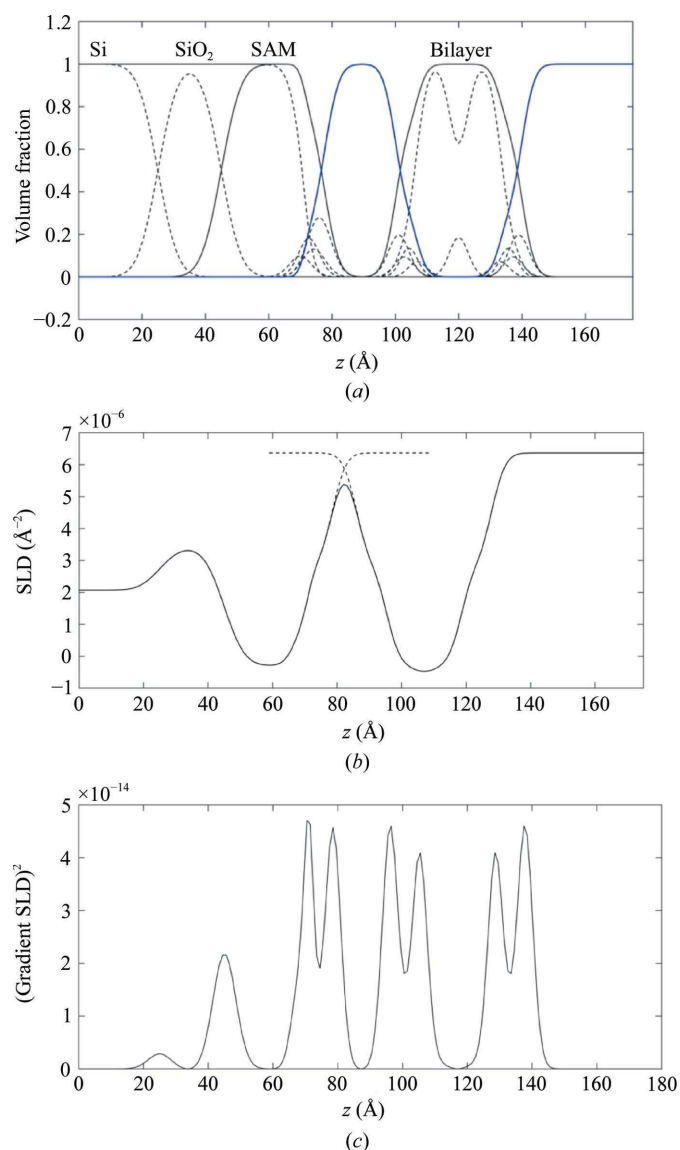


Figure 3
(a) The dotted lines show the volume fraction across the entire interface, including contributions from the bilayer components, but also those of the substrate layers and the SAM. The solid black lines show the summed total occupied volume across the interface. The blue line shows the remaining unoccupied volume, which is filled with water. (b) shows a complete SLD profile constructed using volumetric constraints, which results in a continuous profile with no discontinuities, as seen from the squared gradient shown in (c).

$C_B = 1$, and the dashed-dotted line again shows the original profile, but with a roughness of 2 Å and $C_B = 0.75$.

3.2. An example: fluid DPPC

As an example, we apply both the ‘full simulation’ method described in the previous section and also the CSR method to a typical neutron reflection data set from a DPPC floating bilayer. The membrane is as described previously, supported on a thiolipid SAM on a gold substrate (Hughes *et al.*, 2014), with a magnetic permalloy underlayer. Measuring the system using polarized neutrons and a magnetizable underlayer then results in a different value for the alloy SLD depending on whether the interface is measured with neutron spins parallel or antiparallel to the direction of magnetization of the alloy, giving two separate ‘magnetic contrasts’ (Hughes *et al.*, 2014). The membrane was measured at 50°C, and thus in the ‘fluid phase’ of the bilayer. Additionally, the system was measured against D₂O and H₂O, giving four simultaneous contrasts in total, and the resulting data are shown in Fig. 5(a).

3.2.1. ‘Full simulation’ model. The model described in the previous section, using a DPPC bilayer simulation obtained as described in §2, was fitted to the data using a Bayesian approach, with the fitted membrane parameters being the bilayer centre position, D_B , the bilayer fluctuation roughness, R_B , and the bilayer fractional coverage, C_B . In addition, the thickness of the metal layer, SLDs and roughness, and the SAM parameters (area per molecule, roughness and centre positions of the SAM Gaussians) are also fitting parameters, resulting in 17 parameters in total. The best fitting SLD profiles are shown in Fig. 5(b), with the solid lines in Fig. 5(a) being the reflectivities calculated from the values given in Table 1. In both Figs. 5(a) and 5(b) the shading around each set of curves shows the 95% Bayesian prediction intervals calculated from the ‘minimum’ and ‘maximum’ ranges of the parameter values. The posterior distributions and cross-correlations for the bilayer parameters are also shown in Fig. 5.

As can be seen, the correspondence between model and experiment is excellent, with the best fit going through each

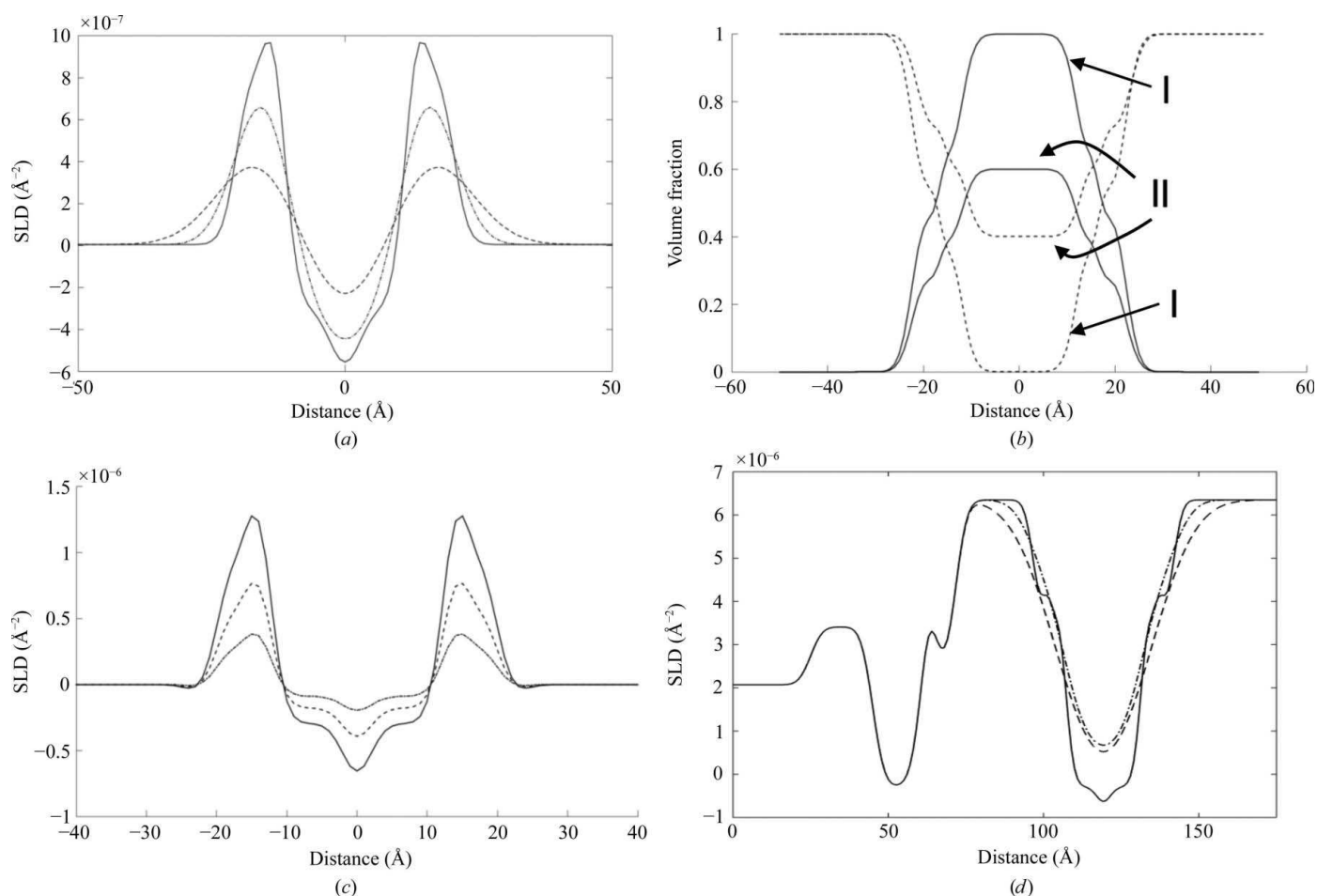


Figure 4

(a) Effect of a Fourier convolution of an SLD profile with a Gaussian to simulate out-of-plane membrane displacements. The ‘as-calculated’ profile is shown convoluted with Gaussians of 2 Å (dashed-dotted line) and 7 Å (dashed line). (b) Correction of the volume fraction to account for reduced coverage of the membrane. The solid lines show the total volume fraction of the membranes, and the dotted lines show the resulting water distributions. The pair labelled ‘I’ show full occupancy and that labelled ‘II’ show the effect of $C_B = 0.6$. (c) Effect of scaling the calculated SLD profile with $C_B = 0.7$ (dashed line) and $C_B = 0.3$ (dashed-dotted line). (d) Full profile obtained using the model with $C_B = 1$ and $R_B = 1$ Å (continuous line), $C_B = 0.9$ and $R_B = 8$ Å (dashed-dotted line) and $C_B = 0.7$ and $R_B = 3$ Å (dashed line).

error bar simultaneously across all four curves over the entire q_z range of the measurement. The posterior distributions of the three membrane parameters along with their cross-correlations are also shown in Fig. 5. In this sample, the best agreement between theory and experiment requires a membrane coverage of around 90%, with a fluctuation roughness of 2 Å. The thickness of the central water cushion is 28 Å.

3.2.2. CSR model. In the method discussed in the previous sections, we incorporate the results of the whole MD simulation directly into the construction of the SLD profile, but an

alternative approach that has been often used is to build the model from functional forms (usually Gaussians); in other words, extending the approach used to model the SAM in the previous sections to the whole membrane.

The main difference between the models is that rather than being extracted directly from the simulations according to (1), the head-group probability distributions are instead modelled as Gaussians, with the submolecular grouping as those in Fig. 1 (*i.e.* four Gaussians per head group). The central methyl region is also represented by a Gaussian, as described previously. The alkyl region is represented by a ‘step’ function

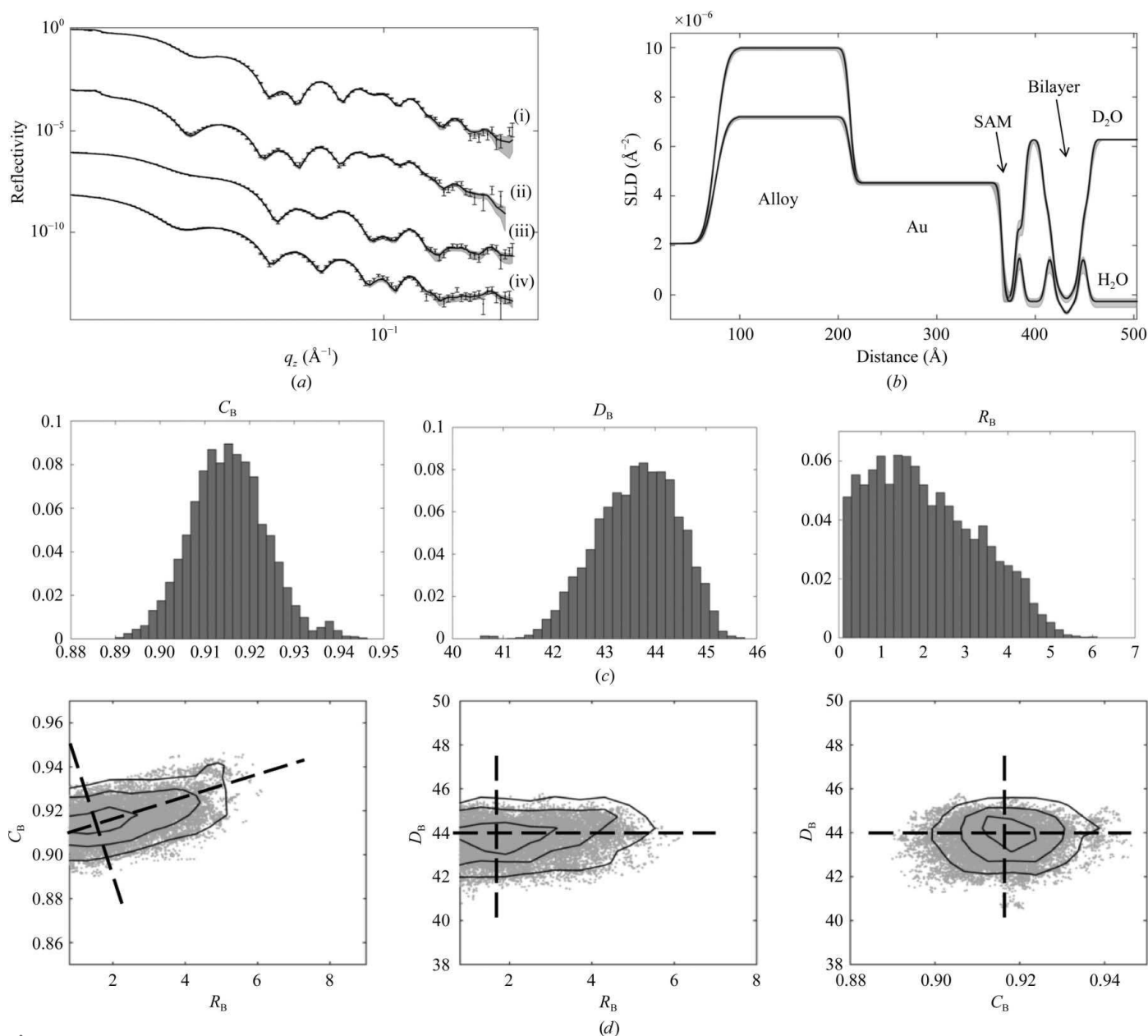


Figure 5 (a) Polarized neutron reflection data from a DPPC floating bilayer. Magnetic contrasts are used, and the sample is measured against both D_2O and H_2O , leading to four contrasts in total. Contrasts (i) and (ii) are D_2O at the two spin states, whilst (iii) and (iv) are those against H_2O . The solid lines are the simultaneous best fit of the model to the four contrasts, and the shading shows the 95% prediction intervals for the parameter values given in Table 1. (b) SLD profiles corresponding to the fits in (a). (c) Posterior distributions and (d) correlation plots for the three bilayer parameters, R_B (the bilayer roughness), C_B (the bilayer coverage) and D_B , which is defined as the distance from the centre of the SAM head group to the centre of the bilayer.

Table 1

Best-fit parameter values for the fit shown in Fig. 5.

Parameter	Value (min, max)	Priors
Substrate roughness (Å)	8.76 (8.045, 9.490)	Uniform (min = 3, max = 12)
Alloy thickness (Å)	136.45 (135.93, 137.01)	Uniform (min = 100, max = 200)
Alloy SLD spin up (Å ⁻²)	9.98×10^{-6} (9.92×10^{-6} , 1.0×10^{-5})	Uniform (min = 9×10^{-6} , max = 1.2×10^{-5})
Alloy SLD spin down (Å ⁻²)	7.19×10^{-6} (7.13×10^{-6} , 7.25×10^{-6})	Uniform (min = 5×10^{-6} , max = 9×10^{-6})
Alloy roughness (Å)	4.08 (3.12, 5.34)	Uniform (min = 3, max = 8)
Gold thickness (Å)	154.16 (153.58, 154.77)	Uniform (min = 100, max = 200)
Gold roughness (Å)	2.81 (1.15, 4.55)	Uniform (min = 1, max = 7)
Gold SLD (Å ⁻²)	4.53×10^{-6} (4.47×10^{-6} , 4.58×10^{-6})	Uniform (min = 4×10^{-6} , max = 5×10^{-6})
SAM coverage	0.99 (0.97, 1.0)	Uniform (min = 0, max = 1)
SAM APM (Å ²)	45.66 (43.59, 47.79)	Uniform (min = 40, max = 90)
$Z_{\text{Carb-Gly}}^{\text{SAM}}$ (Å)	0.66 (0.11, 2.10)	Uniform (min = 0.1, max = 5)
$Z_{\text{Gly-PO4}}^{\text{SAM}}$ (Å)	0.92 (0.12, 2.75)	Uniform (min = 0.1, max = 5)
$Z_{\text{PO4-Chol}}^{\text{SAM}}$ (Å)	1.17 (0.14, 3.10)	Uniform (min = 0.1, max = 5)
SAM roughness (Å)	3.56 (2.71, 4.39)	Gaussian ($\mu = 4$, $\sigma = 0.5$)
Bilayer coverage	0.92 (0.90, 0.93)	Uniform (min = 0, max = 1)
Bilayer position (D_B)	43.64 (42.04, 45.01)	Uniform (min = 20, max = 140)
Bilayer roughness (R_B)	2.06 (0.20, 4.58)	Uniform (min = 0.1, max = 12)

Table 2

Best-fit parameter values from applying the CSR model to the same data as in Fig. 5.

Only bilayer parameters are shown, with the results for the SAM and lower layers being very similar to those in Table 1. The second column shows the values and 95% prediction intervals with no priors, whilst the final column shows the same values obtained with the priors from column 3.

Parameter	Values (min, max) without priors	Priors	Values with priors
Bilayer roughness (Å)	0.28 (0.0182, 0.779)	Uniform (min = 0.1, max = 12)	4.9 (0.25, 9.76)
Bilayer APM (Å ²)	68.71 (51.44, 87.54)	Uniform (min = 48, max = 90)	69.2 (57.4, 79.3)
Z_{Gly} (Å)	5.52 (0.42, 9.79)	Gaussian ($\mu = 4.2$, $\sigma = 0.4$)	4.17 (3.32, 5.30)
Z_{PO4} (Å)	6.04 (0.41, 9.79)	Gaussian ($\mu = 4.86$, $\sigma = 0.6$)	4.96 (3.86, 5.83)
Z_{Chol} (Å)	6.63 (2.51, 9.63)	Gaussian ($\mu = 5.33$, $\sigma = 0.6$)	5.6 (4.67, 6.50)
A_{CH3} (Å)	5.21 (1.22, 9.75)	Gaussian ($\mu = 5.3$, $\sigma = 0.6$)	5.2 (4.44, 6.29)
A_{Carb} (Å)	3.08 (1.09, 5.73)	Gaussian ($\mu = 4.1$, $\sigma = 0.6$)	3.99 (3.17, 4.97)
A_{Gly} (Å)	5.55 (1.22, 9.74)	Gaussian ($\mu = 4.3$, $\sigma = 0.6$)	3.85 (2.86, 4.75)
A_{PO4} (Å)	5.73 (1.26, 9.77)	Gaussian ($\mu = 4.1$, $\sigma = 0.6$)	4.01 (3.04, 5.01)
A_{Chol} (Å)	7.02 (1.67, 9.89)	Gaussian ($\mu = 4.2$, $\sigma = 0.6$)	4.4 (3.49, 5.35)

(really two error functions separated by a distance corresponding to the layer thickness), and this is then taken as the volume fraction of the chains. To prevent ‘overfilling’ in the head-group region, we penalize the fit χ^2 as shown previously (Schalke & Lösche, 2000; Schalke *et al.*, 2000), so that the overall fitting χ^2 is given by

$$\chi^2 = \chi^2 + \exp(DX), \quad (5)$$

where D is a scaling parameter ($D = 100$ in this work), and

$$X = \frac{1}{N} \sum_{i=1}^N \left[\sum_{\xi} P_{\xi}(z) - 1 \right]^2. \quad (6)$$

Fig. 6(a) shows the bilayer SLD profiles obtained from each model against H₂O, with the MD results shown in blue and the CSR structure in green. The accompanying probability distributions are shown in Fig. 6(b), with the dotted lines from the MD simulation and the solid lines the result of the CSR fit. The shaded 95% prediction interval shown around the MD structure is the result of applying the coverage and roughness corrections to the simulated structure, whilst that of the CSR fit is the result of fitting Gaussian positions and widths, in addition to roughness and coverage. Clearly, the CSR model

as fitted here does not retrieve the true membrane structure, with the best-fit structure shown by the solid green line differing significantly from the structure obtained from modelling (blue line). There is also very considerable uncertainty around the result, with the 95% prediction envelope showing a broad variability around the fit. The probability distributions of the fragment positions from CSR were obtained from the best-fit values (from the second column of Table 2).

The reason for its poor performance becomes apparent if the posterior distributions of the individual structural parameters are examined. These are shown by the red distributions in Fig. 6(e), and all of the posteriors for the head-group Gaussians (A_{ξ} and Z_{ξ}) are exceedingly broad, so much so that the individual parameters are effectively undefined. Similarly, the posterior distribution of the lipid area per molecule (APM) is also very broad. In practice, therefore, no real conclusions can be drawn regarding the submolecular organization of the membrane from CSR as run here on this data set.

The analysis in Figs. 6(a) and 6(b) was run using the conventional information input into the CSR model of just the fragment volumes. If we also include information regarding

fragment distributions by setting Gaussian priors on fragment positions and widths (solid lines in Fig. 6*e*), then CSR is seen to perform far more robustly. The resulting posterior histograms, which were obtained using the priors in the third column of Table 2, are shown in blue in Fig. 6*e*. The priors were chosen by inspection so that the distributions closely match those obtained from the simulation (*i.e.* to reproduce Fig. 1*c*). Fig. 6*c*) shows the same comparison as Fig. 6*a*) for the weighted fit, and there is clearly far better agreement between CSR and simulation for this more constrained structure, and the prediction interval surrounding the best-fit line is also substantially reduced. There also is far better agreement with the simulated structure, as can be seen from Fig. 6*d*).

4. Discussion

We have applied two methods for introducing information from molecular modelling into reflectivity analysis to a neutron reflection data set from a DPPC bilayer. In the first method we take the entire simulation, convert this into an

SLD, and then use this to fit the measured data. In the second approach, we (initially) take only the component volumes from the simulation as the input to the modelling, and construct the SLD profile in a structural form. The former is often referred to as a ‘static’ approach, since the result of the simulation is unmodified by the data analysis, and therefore it is a comparison between the simulation result and measured data only. The latter approach of using functional forms is an example of a ‘dynamic’ approach, in which the aim is to use free-fitting of functional representations of the membrane to recover a membrane structure, which can then subsequently be compared with the simulation. Thus, in principle the dynamic approach can be used to analyse analogous samples (such as lipids with the same head group but different chain lengths, for example) without the need for another simulation. For the static approach a fresh simulation is required for each sample.

The two key points from our implementation of the static approach are firstly that constructing the whole interfacial

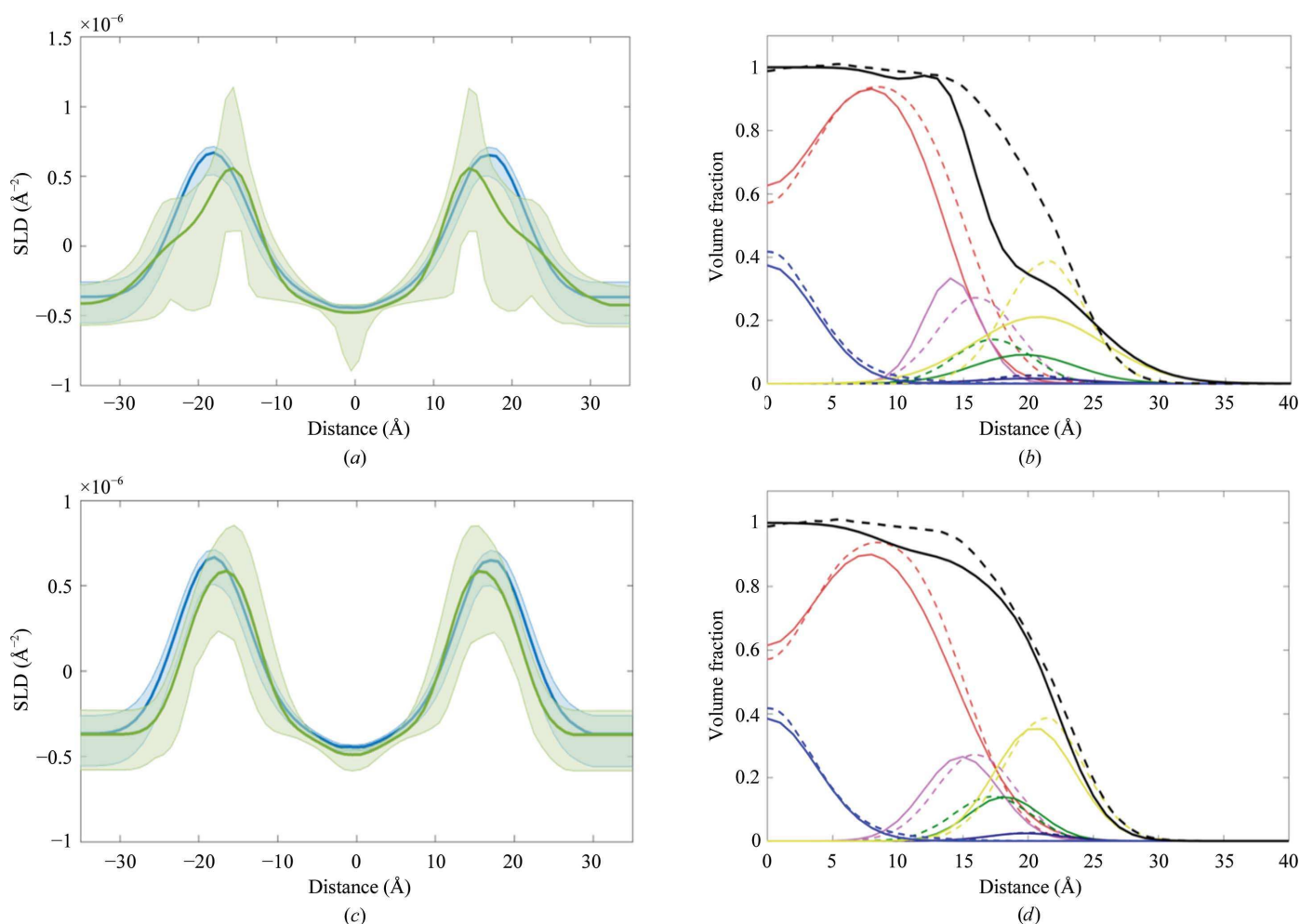


Figure 6
(*a*) Comparison between the SLD profiles from unconstrained CSR (green) and the whole-simulation MD (blue). Shaded regions are the 95% prediction intervals from the Bayesian analysis. CSR does not accurately reproduce the membrane structure in this case, as is clear from the comparison of probability distributions shown in (*b*). Solid lines are CSR distributions, dotted lines are from CSR and the parameter posterior distributions are shown as red histograms in (*e*). Also shown in (*e*) are the parameter distributions obtained with Gaussian priors on parameters, shown as black lines (where used); the resulting posterior histograms are shown in blue. This improves the correlation between the CSR and MD structures, as shown in (*c*) and (*d*).

profile (*i.e.* the bilayer plus supporting layers) in terms of number densities and occupied volumes, rather than by joining together individual SLD curves, removes any discontinuities caused by splicing errors, and hence prevents artefacts encroaching into the calculation of the resulting reflectivities. Secondly, the approach accounts for the fact that an MD simulation of a membrane is not itself sufficient to describe the structure that will actually be measured in a real-world measurement, since out-of-plane displacements over and above those seen in a finite, small-scale simulation will most likely be present, and also defects will usually exist (leading to reduced coverage), and corrections must be applied to the MD-derived structures to account for these effects.

For the case of the DPPC example shown here, there is a very good correspondence between model and experiment with the static model, with the fit going through every point simultaneously across four contrasts. A Bayesian analysis shows that the bilayer parameters are orthogonal except for between the membrane roughness and coverage, where some correlation exists. This is not surprising given the similar effect both can have on the SLD profile, as is illustrated in Fig. 4(*d*), where a membrane of full coverage but large roughness results in a similar overall profile to a lower coverage membrane of lower roughness. The extracted roughness value of about 2 Å

suggests that only a small correction is required for fluctuations in this example, and the displacement is largely accounted for by the existing displacements arising from the simulation itself. However, this is not always the case, and under some conditions membrane fluctuations can increase dramatically when interactions lead to large changes in the membrane bending modulus. These correlations should therefore be kept in mind and examined, and if required the fluctuation amplitude can be measured independently (Dailant *et al.*, 2005). However, the dynamic CSR approach, when applied as is conventionally performed using only component volumes as an input, performs very poorly and fails to recover the simulated membrane structure. It is only when additional information is provided in the form of priors on head-group component positions and widths that the membrane structure is convincingly obtained.

The dynamic CSR approach is the method that has most often been applied to the analysis of SANS and diffraction data, and in both those cases a significantly larger data set was required for a full structural determination. Thus, for example, Kučerka and coworkers considered small-angle scattering data from both DOPC and DPPC, and in both cases multiple samples measured (by neutrons) at multiple solvent deuterations, but also at several partial sample deuterations, and also

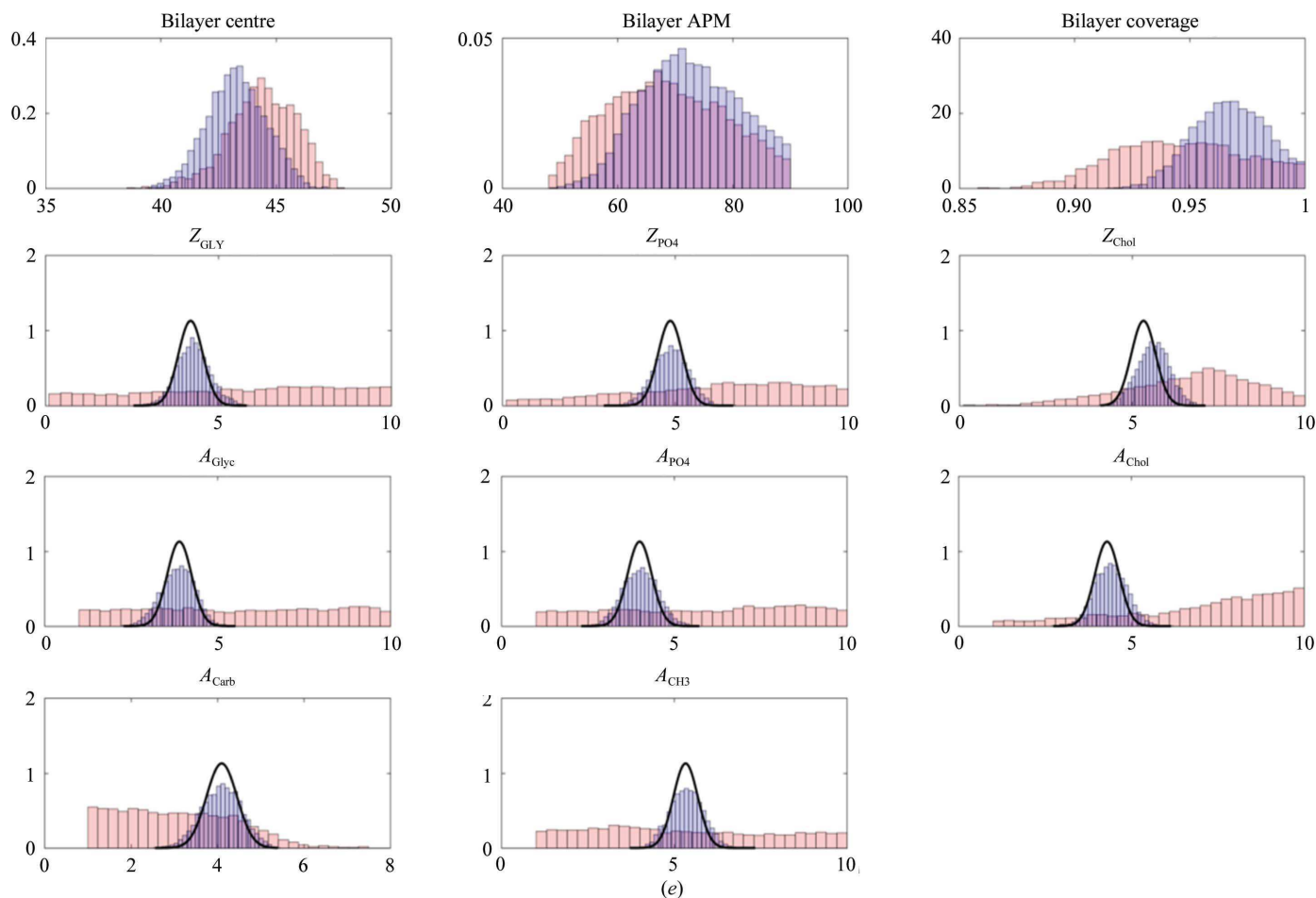


Figure 6 (continued)

including an X-ray contrast, were fitted simultaneously (Kučerka *et al.*, 2008, 2012). For diffraction, Wiener and White employed a similar simultaneous analysis of a broad range of deuterations along with an X-ray contrast (Wiener & White, 1992). It is therefore perhaps not surprising that reflectivity performs so poorly when applied to this data set of a single deuteration only, since there is insufficient inherent information content in this small data set and the model is too over-determined to recover fragment positions and widths accurately. It is likely that if a simultaneous analysis of multiple samples each at different specific deuterations and water contrasts (and perhaps also including an X-ray contrast) were included in the reflectivity analysis then the posteriors would become far better defined and the membrane structure better determined. However, access to neutron and X-ray scattering is usually limited, and detailed data sets with systematic variation in specific deuteration are the exception rather than the norm. In most experiments the limited data set used here is far more usual, and indeed, for most lipids outside the 'usual suspects' (such as DPPC or POPC), selectively deuterated lipids are difficult to obtain commercially. In such cases, the more limited data sets of the type shown here are the only available option.

In the absence of additional data, more information can be supplied to the CSR fit from modelling by specifying both positions and widths more closely, in addition to supplying component volumes, which we perform here by setting Bayesian priors on the relevant parameters. CSR then performs far more robustly, recovering the modelled structure reasonably well, but even then still struggles to recover other unknown membrane properties of interest. Thus, for example, a key parameter of interest in biophysical studies is the projected area per lipid molecule (APM). Kučerka and coworkers report a value of 63.1 \AA^2 for DPPC, which is in good agreement with simulation. As can be seen from Fig. 6(e), even with constrained fragment positions the 95% confidence interval on the fitted value of the APM is between 57.2 and 71.1 \AA^2 , so although the published values of the area lie within this range, it is clearly not well determined by CSR on this limited data set. [It should be noted that the slight differences between the fragment distributions which remain in Fig. 6(d) are substantially owing to the still poor definition of APM, and the correspondence between the CSR and simulated distributions would improve further if an additional prior were set for the lipid area.]

In the case of the static approach, the APM is of course completely defined by the simulation, and this highlights the key difference between the two approaches. All decisions regarding the membrane structure are passed to the simulation side rather than the data-fitting side, and the data analysis itself is then just a comparison of the simulation with the measured data. This method is therefore of main use for 'screening' potential models for corroboration by experiment, where more than one structural possibility exists. Thus, for example, if more than one orientation of a membrane protein might be in principle be possible based on simulations, then in that case comparison between theory and experiment using

this method would allow possible simulation results to be examined in order to determine which are the most appropriate structures.

The stated advantage of CSR is so that information obtained from MD simulations can be used interchangeably for systems other than those simulated, thus removing the need to carry out new simulations for each system studied. Therefore, from a simulation of DPPC, for example, one can extract the component volumes, and if the assumption is made that these change little in different environments (and as we have shown, if a sufficiently detailed data set is available), then these could then be used to analyse data from more complicated mixed films where DPPC is a component. This is of course still the case, and when no simulation of the system under study exists it is indeed the only feasible approach. However, these results show that great care must be taken not to overdetermine the problem, and that in some cases that extracting only volumetric information from the simulations is insufficient for an accurate analysis.

For more complicated systems, particularly those containing proteins, an additional problem of CSR is that the *a priori* selection of a functional form to represent each of the fragments may also become more challenging. For the case of DPPC, the fragment distributions from the simulation are almost perfect Gaussians, and thus this is not such a difficulty. For more complicated components, such as proteins or lipopolysaccharides for example, this is unlikely to be the case. In the case of proteins, methods have been proposed where the protein is simulated in isolation, an SLD 'envelope' is extracted and this then superimposed on a membrane signal, usually constructed from a standard layer model (Heinrich & Lösche, 2014). As the original authors point out, there are several potential issues with this approach. Simulating the protein outside the membrane environment may lead to a different structure for the peptide than when embedded; operator choices must be made about likely orientations in the membrane, again leading to modelling bias (although in some cases orientation parameters can be defined), and also the effect of the protein on the immediate membrane environment is not simulated.

The static method, however, also offers a way to resolve these problems. In practical terms, simulating proteins and the associated membrane patch is now very feasible, although an extra correction is required in order to use these simulations in this approach, in that the simulations will not always be of the correct protein:lipid ratio for the data. In such cases, the SLD envelope used will simply be a scaled average of protein-containing membrane and a 'pure' bilayer simulation to reflect the appropriate protein loading of the sample in the beam area if it is lower than the simulation, or a simple truncation of the simulation box if the loading of the simulation is too low.

However, the central point of this article is that although both static and dynamic methods are capable of describing reflectivity data, and each approach has caveats and advantages, the range of applicability depends on the quality of the data available. For sparse data sets consisting perhaps of a single sample measured at a series of solvent deuterations,

then this is insufficient to merit the full dynamic approach. In such cases then it is more appropriate to transfer the burden of the structural determination to the simulation side, and to then use data analysis as a validation of the simulated structure. Where more detailed data are available, then dynamic approaches become progressively more applicable. In either case, it is always necessary to examine the uncertainties in model fits in some detail to avoid overdetermining analyses, whichever approach is used.

5. Conclusions

A method for producing continuous SLD profiles from molecular-dynamics simulations has been presented for interpreting reflectivity data from lipid bilayers. The method avoids introducing artefacts caused by poor splicing between the MD SLD and the model representing the rest of the interface by splicing in terms of occupied volume, rather than in terms of SLD. In the simple example of DPPC, the experimental data can be replicated simultaneously across multiple neutron contrasts once corrections have been made for coverage and out-of-plane membrane deformations. The method has the advantage of removing operator bias from the modelling of complex membrane environments, therefore aiding the screening of MD structures by comparison to experimental data.

Acknowledgements

This research has been supported by the European Commission under the Seventh Framework Program through the ‘Research Infrastructures’ action of the ‘Capacities’ Program, NMI3-II Grant No. 283883. ACK and MSPS were supported by the Wellcome Trust. Computing resources were provided by STFC Scientific Computing Department’s SCARF cluster.

References

Abeles, F. (1950). *J. Phys. Radium*, **11**, 307–310.
 Armen, R. S., Uitto, O. D. & Feller, S. E. (1998). *Biophys. J.* **75**, 734–744.
 Bussi, G., Donadio, D. & Parrinello, M. (2007). *J. Chem. Phys.* **126**, 014101.
 Clifton, L. A., Holt, S. A., Hughes, A. V., Arunmanee, W., Heinrich, F., Khalid, S., Jefferies, D., Charlton, T. R., Webster, J. R. P., Kinane, C. J. & Lakey, J. H. (2015). *Angew. Chem. Int. Ed. Engl.* **54**, 11952–11955.
 Dabkowska, A. P., Michanek, A., Jaeger, L., Rabe, M., Chworos, A., Höök, F., Nylander, T. & Sparr, E. (2015). *Nanoscale*, **7**, 583–596.

Daillant, J., Bellet-Amalric, E., Braslau, A., Charitat, T., Fragneto, G., Graner, F., Mora, S., Rieutord, F. & Stidder, B. (2005). *Proc. Natl Acad. Sci. USA*, **102**, 11639–11644.
 Darden, T., York, D. & Pedersen, L. (1993). *J. Chem. Phys.* **98**, 10089.
 Darré, L., Iglesias-Fernandez, J., Kohlmeyer, A., Wacklin, H. & Domene, C. (2015). *J. Chem. Theory Comput.* **11**, 4875–4884.
 Daulton, E. (2015). PhD thesis. University of Bath.
 Fragneto, G., Charitat, T. & Daillant, J. (2012). *Eur. Biophys. J.* **41**, 863–874.
 Haario, H., Laine, M., Mira, A. & Saksman, E. (2006). *Stat. Comput.* **16**, 339–354.
 Heinrich, F. & Lösche, M. (2014). *Biochim. Biophys. Acta*, **1838**, 2341–2349.
 Helfrich, W. (1973). *Z. Naturforsch. C*, **28**, 693–703.
 Hess, B., Bekker, H., Berendsen, H. J. C. & Fraaije, J. G. E. M. (1997). *J. Comput. Chem.* **18**, 1463–1472.
 Hughes, A. V., Holt, S. A., Daulton, E., Soliakov, A., Charlton, T. R., Roser, S. J. & Lakey, J. H. (2014). *J. R. Soc. Interface*, **11**, 20140447.
 Hughes, A. V., Howse, J. R., Dabkowska, A., Jones, R. A., Lawrence, M. J. & Roser, S. J. (2008). *Langmuir*, **24**, 1989–1999.
 Hughes, A. V., Roser, S. J., Gerstenberg, M., Goldar, A., Stidder, B., Feidenhans'l, R. & Bradshaw, J. (2002). *Langmuir*, **18**, 8161–8171.
 Kaszuba, K., Grzybek, M., Orłowski, A., Danne, R., Róg, T., Simons, K., Coskun, Ü. & Vattulainen, I. (2015). *Proc. Natl Acad. Sci. USA*, **112**, 4334–4339.
 Katsaras, J. & Gutberlet, T. (2001). Editors. *Lipid Bilayers: Structure and Interactions*. Berlin: Springer.
 Koldsø, H., Shorthouse, D., Hélié, J. & Sansom, M. S. P. (2014). *PLoS Comput. Biol.* **10**, e1003911.
 Kučerka, N., Holland, B. W., Gray, C. G., Tomberli, B. & Katsaras, J. (2012). *J. Phys. Chem. B*, **116**, 232–239.
 Kučerka, N., Nagle, J. F., Sachs, J. N., Feller, S. E., Pencer, J., Jackson, A. & Katsaras, J. (2008). *Biophys. J.* **95**, 2356–2367.
 Kukul, A. (2009). *J. Chem. Theory Comput.* **5**, 615–626.
 Majewski, J., Wong, J. Y., Park, C. K., Seitz, M., Israelachvili, J. N. & Smith, G. S. (1998). *Biophys. J.* **75**, 2363–2367.
 Marrink, S. J., Risselada, H. J., Yefimov, S., Tieleman, D. P. & de Vries, A. H. (2007). *J. Phys. Chem. B*, **111**, 7812–7824.
 Parrinello, M. & Rahman, A. (1981). *J. Appl. Phys.* **52**, 7182–7190.
 Penfold, J. (2002). *Curr. Opin. Colloid Interface Sci.* **7**, 139–147.
 Petrache, H. I., Feller, S. E. & Nagle, J. F. (1997). *Biophys. J.* **72**, 2237–2242.
 Richter, R. P., Bérat, R. & Brisson, A. R. (2006). *Langmuir*, **22**, 3497–3505.
 Sachs, J. M. & Engelman, D. M. (2006). *Ann. Rev. Biochem.* **75**, 707–712.
 Schalke, M., Krüger, P., Weygand, M. & Lösche, M. (2000). *Biochim. Biophys. Acta* **1464**, 113–126.
 Schalke, M. & Lösche, M. (2000). *Adv. Colloid Interface Sci.* **88**, 243–274.
 Tristram-Nagle, S., Petrache, H. I. & Nagle, J. F. (1998). *Biophys. J.* **75**, 917–925.
 Wacklin, H. P. (2010). *Curr. Opin. Colloid Interface Sci.* **15**, 445–454.
 Wiener, M. C. & White, S. H. (1992). *Biophys. J.* **61**, 434–447.
 Xing, C. & Faller, R. (2008). *J. Phys. Chem. B*, **112**, 7086–7094.